ACS Photonics

pubs.acs.org/journal/apchd5

Article

Graphene-Based Tunable Coloration Film through Intercalation

Ganying Zeng, Renyan Zhang,* Yinlong Tan, Xiang'ai Cheng, and Tian Jiang*

Cite This: https://doi.org/10.1021/acsphotonics.1c01223

Read Online

ACCESS | Metrics & More | Article Recommendations | Supporting Information

ABSTRACT: Optical materials with dynamic colors have shown great prospects for applications in display devices, smart windows, and camouflage coatings. Recently, intercalation has been demonstrated to be a powerful strategy for tuning electromagnetic properties of two-dimensional materials ranging from visible to microwave wavelengths, such as the visible color, infrared emission, terahertz radiation, and optical second-harmonic generation. Here, a systematic study of graphene intercalation compound (GIC)-based coloration films is presented. Through lithium (Li), sulfuric acid (H_2SO_4), and ferric chloride ($FeCl_3$) intercalation, the color of a multilayer graphene (MLG) film transforms from gray to yellow, blue, and dark, respectively. This is attributed to the reconstruction of the band structure of graphene after intercalation, resulting in a significant effect on its optical properties. Furthermore, tunable and reversible color changes of MLG film have been demonstrated by precisely controlling the Li-intercalation process. Our research indicates that intercalation is a versatile strategy for fabricating advanced coloration materials and provides a promising tunable optical surface for the application in sensing, adaptive camouflage, and smart displaying.

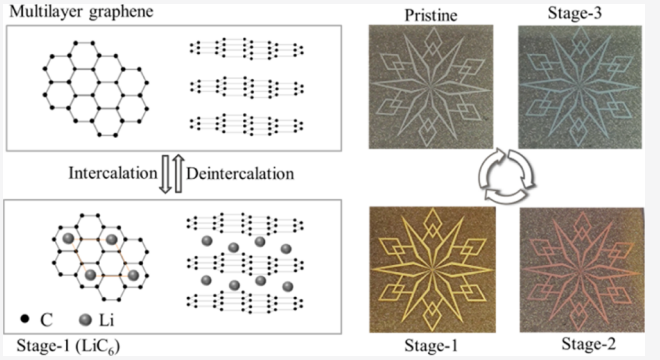

KEYWORDS: *multilayer graphene, intercalation, tunable, coloration film, optical reflectance*

INTRODUCTION

Dynamic color manipulation is vital in extensive applications, such as display devices,[1] smart window,[2] camouflage engineering,[3] and optical sensors.[4] Organic pigments including printing inks and paints are the convenient coloration materials used for color generation. However, it still has some unavoidable drawbacks such as insufficient resolution,[5,6] poor stability, and difficult tunability.[7,8] Thus, the tuning methods such as electrochromic, thermochromic, and photochromic are proposed for dynamic color manipulation.[9−11] Liu et al. developed a nontoxic chlorophenol red−water thermochromic system for clear and reversible color display.[9] Yang et al. provided photochromic nanocomposite organohydrogels with high transparency, excellent strength, and 60 s response time.[10] Meanwhile, structural color is another important approach to produce high-resolution colors with a physical structure.[12,13] By designing nanostructures such as nanowires,[14] gratings,[15] and disk-hole coupling[16] with suitable geometrical parameters, the desired color can be acquired from reflecting or scattering light through periodic arrays or individual resonators.[14,15] By combining advantages of the structural color and smart materials such as electrochromic materials, many researchers have shown excellent works about color tuning.[17−22] For example, Arsenault et al. reported an electrical control method to control photonic crystals to fabricate a full-color display with 1−2 s response time, and its cycling stability is excellent.[23] Lee et al. showed a novel dynamic structural color based on organic electrochromic materials. The vivid and high-contrast color can be generated under an electrochemical bias with a response time of 40 s.[24]

Intercalation provides a unique ability to manipulate light−matter interactions in two-dimensional (2D) materials by inserting ions, molecules, metals into their van der Waals gap interlayer.[25−27] The fascinating area of intercalation is leading to numerous novel phenomena such as superconductivity,[28] ferromagnetism,[29] phase transition,[30] and charge density wave.[31] What needs to be emphasized is that distinctive optical responses have also been observed during the intercalation process. The absorbance of broad wavelengths can be dramatically changed by intercalation. A sandwiched thin films containing carbon nanotubes and reduced graphene oxide has a transmittance increase by about 20−30% for 20 layers with the spectral wavelength ranging from the visible to the infrared via Li intercalation.[32] Upon ionic liquid intercalation, the infrared emissivity could be tuned from 0.57 to 0.41 in graphene films,[33] which can realize a fast and controlled infrared camouflage on an active thermal graphene

Received: August 11, 2021

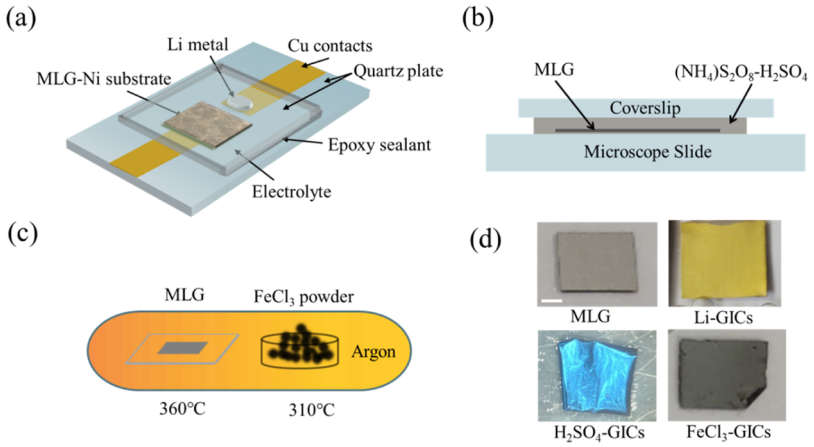

Figure 1. Experimental schematics of MLG intercalation compounds preparation. (a) Experimental setup of planar battery devices for electrochemical tuning Li intercalation and in situ optoelectronic measurements. MLG CVD-grown on a Ni foil is contacted with a quartz substrate. (b) Experimental setup of the optical cell for chemical tuning H_2SO_4 intercalation and in situ optical measurements. A MLG film contacted with a quartz substrate. (c) Experimental setup of the two-zone vapor transport method for intercalating $FeCl_3$ into MLG films. A MLG film contacted with a quartz substrate. (d) Optical images of pristine MLG before and after Li, H_2SO_4, and $FeCl_3$ intercalation. The scale bar is 2 mm.

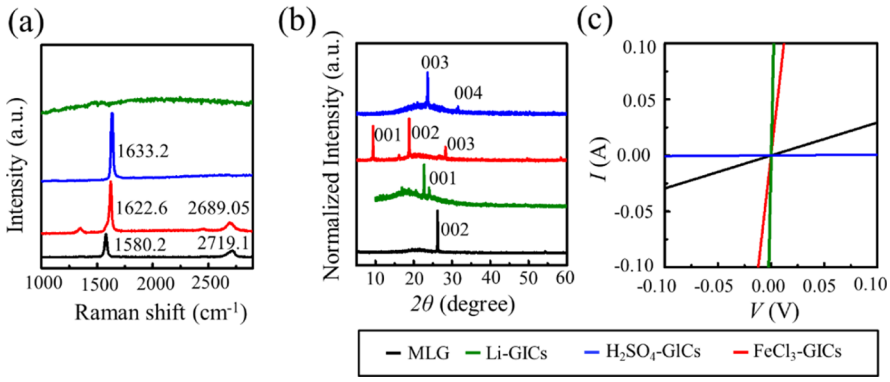

Figure 2. (a−c) are Raman spectra, XRD patterns, and four-probe $I-V$ curves of pristine MLG before and after Li, $FeCl_3$, H_2SO_4 intercalation. The black line represents pristine MLG with no intercalation. Green, blue, and red solid lines represent pristine MLG with Li, H_2SO_4, and $FeCl_3$ intercalation, respectively.

film.[34] In addition, a reversible and tunable nonlinear optical second-harmonic generation signal is found in ultrathin graphite flakes due to inversion symmetry breaking via the Li intercalation.[35] Very recently, a transformation from saturated absorption to reverse saturation absorption can be realized in few-layer graphene through Li intercalation.[36] However, the color control method based on 2D materials and intercalation is rarely reported, which has the potential to realize a continuous dynamic color manipulation in a macroscale area by a simple fabrication process.[25]

In this work, we present a color-changing multilayer graphene (MLG) film through intercalation. Li, H_2SO_4, and $FeCl_3$ intercalation could change the color of graphene coloration film from gray to bright yellow, deep blue, and dark, respectively. With precise manipulating of the reversible lithiation/delithiation behavior, consecutive and cyclic colors are present in a broad visible band. Moreover, LiC_6 displays good stability without applied voltage for both the color and reflectivity spectrum. To further demonstrate the potential application of this technique, a school logo with a dynamic color of the National University of Defense Technology is presented. Our result provides a simple and effective method to dynamically tune 2D materials' coloration.

RESULT AND DISCUSSION

Figure 1 illustrates the sample fabrication process. Figure 1a shows a planar battery configuration, we design a sandwich-structured cell with an electrolyte ($LiPF_6$ in ethylene carbonate/diethyl carbonate, w/w = 1:1). The device is sealed between the bottom and top quartz plate to prevent oxidation. Chemical vapor deposition (CVD)-grown large-area MLG on a nickel (Ni) foil and the Li source is deposited on the bottom quartz plate and is connected to two separate copper (Cu) contacts. In this planar battery, the Li metal is used as the counter electrode and MLG as the working electrode. The intercalation process is controlled by an electrochemical workstation, and the voltage is in the range of 3.0−0.05 V versus Li/Li^+ of the planar battery, which can be measured simultaneously during the electrochemical Li intercalation (Figure S1). This platform is used to carry out the optical and electrical property characterization of MLG during Li intercalation in situ. Figure 1b demonstrates another sandwich structure for the H_2SO_4 intercalation of MLG. The MLG is immersed in the $(NH_4)_2S_2O_8-H_2SO_4$ solution, and two glass slides are used to clamp the solution which can reduce the exposure to moisture in the air to prevent the de-intercalation process. Similarly, this device can be characterized in situ.

https://doi.org/10.1021/acsphotonics.1c01223
ACS Photonics XXXX, XXX, XXX−XXX

Figure 1c shows that $FeCl_3$-GICs are synthesized by a traditional two-zone method. Both anhydrous $FeCl_3$ powder and the quartz plate with MLG are positioned in different zones inside a glass tube full of argon. Figure 1d shows the color changes of MLG film by intercalation. For the electrochemical Li intercalation, it displays a consecutive color change and a yellow color for the full intercalation, which spends about 4 and 3 h with a 3 μA constant current corresponding to the first charge and discharge process, as shown in Figure S1. For the H_2SO_4 intercalation, there is a blue color produced with 5 min, and only 1.2 min is needed for the color restoration (see Movie S3 and S4). For the $FeCl_3$ intercalation, a black color is observed after intercalation for about 24 h. The reason for the different time scales of Li, H_2SO_4, and $FeCl_3$ intercalated MLG is due to their different synthetic methods. For electrochemical lithium intercalation with electrochemical oxidation, the response time is strongly related to the current. For H_2SO_4 intercalation with chemical oxidation using ammonium persulfate as the chemical oxidizing agent, the production of GICs can be performed within several minutes.[37] For $FeCl_3$ intercalation with gaseous intercalation, the intercalation process is controlled through temperature, by effectively regulating the vapor pressure of the intercalant, and by controlling the thermodynamics of intercalation; it is a low kinetic process.[38]

Graphite forms structures where one, two, or three graphene layers are sandwiched between the two layers of intercalant. The resulting compounds are referred to as stage-1, stage-2, and stage-3 of GICs. These structures' evolution for the intercalation process is studied using the Raman spectroscopy (Figure 2a). The black line depicts the Raman spectra of pristine MLG films, which show a typical G peak and 2D peak of graphene at 1580.2 and 2719.1 cm^{-1}, respectively. The result is similar to previous research studies.[39] No D peak is found at around 1350 cm^{-1}, which means there are scarce defects in pristine MLG films. After Li intercalated MLG (green line), the G peak and 2D peak completely disappear, corresponding to the formation of stage-1 (LiC_6). This indicates strong doping by charge transfer from Li to graphene layers as to be Pauli-blocked of the inter-band optical transition. Hence, there is no resonant Raman process. The result is consistent with previous research studies.[25,40] In addition, a strong fluorescence background confirms the strong n-type doping after Li intercalation. For $FeCl_3$-GICs (red line), the position of G peak upshifts from 1580.2 to 1622.6 cm^{-1}, with a large blue shift of 42.4 cm^{-1}. This is ascribed to the electronic decoupling effect induced by the layer space increase from graphite to $FeCl_3$. A similar result was also reported in previous studies[41,42] and suggested that the graphene layers were well sandwiched on both sides by $FeCl_3$ monolayers (stage-1). In addition, the 2D peak exhibits a change from a multipeak structure to a single peak and downshifts to monolayer graphene (2689.05 cm^{-1}), further verifying the loss of electronic coupling between adjacent graphene sheets due to the presence of $FeCl_3$. The appearance of the D peak implies that $FeCl_3$ intercalation influences the crystal quality for MLG. For H_2SO_4 intercalated MLG (blue line), G peak upshifts to 1633.2 cm^{-1} position, which is consistent with the previously reported G peak position of stage-1 H_2SO_4-intercalated GICs.[43] The large blue shift (53 cm^{-1}) is due to the charging of carbon layers by the acceptor-type intercalant.[37] There is no 2D peak normally situated at ~2700 cm^{-1} for graphene or graphite, consistent with stage-1.[37] No D peak is around 1350 cm^{-1}, which indicates the crystal quality of MLG maintains well after H_2SO_4 intercalation.

The X-ray diffraction (XRD) pattern can be applied to the analysis of the crystal structure of MLG before and after intercalation (Figure 2b). The pristine MLG characteristic peak's position is at 26.2° (002) and 54.3° (004), corresponding to an interlayer spacing of 3.3 Å. The result is similar to the previous reports.[44] As for the Li-intercalated MLG sample (green line), the diffraction peak position is found at 2θ = 24.0° (001), which shows that the layer space increases from 3.3 Å for graphite to 3.7 Å for LiC_6. This is consistent with the presence of Li atoms between graphene layers.[45] As for MLG intercalated with $FeCl_3$, new peaks appear at 9.4° (001), 18.7° (002), 28.2° (003), which is similar to the previous report of the structure of stage-1 $FeCl_3$-GICs.[44] The lattice spacing is calculated to be 9.4 Å. Nevertheless, the diffraction peak position of H_2SO_4-GICs is found to be at 23.6 and 31.6° between stage-1 and stage-2, according to the previous report.[37] The result seems to be conflicting with the Raman result of this work. This attributes to the non-uniform intercalation process, where the surface of MLG achieves stage-1 but the internal part is still at stage-2. The Raman spectroscopy is a more surface-sensitive technique. In addition, the sharp peaks of XRD imply that their crystal structure remains well after intercalation.

To further characterize the MLG film via intercalation, changes of the sheet resistance are also measured by the van der Pauw method (Figure 2c). The sheet resistance of MLG reduces from 10.2 Ω/sq to 0.224 Ω/sq for Li-GICs, and 1.17 Ω/sq for $FeCl_3$-GICs, but increase to ~782 Ω/sq of H_2SO_4-GICs. According to previous research studies, the resistance of materials will be reduced through intercalation.[25,26] Because intercalation can increase the carrier concentration in the materials, which can increase electrical conductivity.[26] The test results of Li-GICs and $FeCl_3$-GIC are similar to previous reports.[25,26] As to the abnormal behavior of H_2SO_4-GICs, an in situ resistance of MLG film during the H_2SO_4 intercalation process is carried out. The resistance test shows a decrease in the early intercalation process but an increase in the later intercalation process, and a decrease in the de-intercalation process (Figure S2). According to the previous research explanation, a strong decrease of resistivity in the beginning intercalation process can be attributed to the high mobility of positive holes in many graphene layers.[46] The great increase of resistivity in stage-1 is because of the decrease of carrier mobility and overoxidation.[47−49]

To demonstrate the mechanism of intercalation change color, the influence of thickness and substrate on color is investigated, as shown in Figure S3. As a result, the GICs with different thicknesses or those bonded on various substrates show the same yellow color, indicating that the mechanism of intercalation-induced color change is from the material itself. According to the related research studies,[37,50,51] the energy structure of graphene can be significantly changed by intercalation. The Fermi surface of graphene (0 eV) is shifted by 1.5 eV for Li intercalation,[50] ~1.2 eV for H_2SO_4 intercalation,[37] and 1.0 eV for $FeCl_3$ intercalation,[51] respectively. Then, the interband optical transitions for photon energies $\omega < 2E_F$ are suppressed,[25] and the optical bands of graphene changed accordingly. Therefore, optical reflectance is also changed, which is related to the material color.

https://doi.org/10.1021/acsphotonics.1c01223
ACS Photonics XXXX, XXX, XXX−XXX

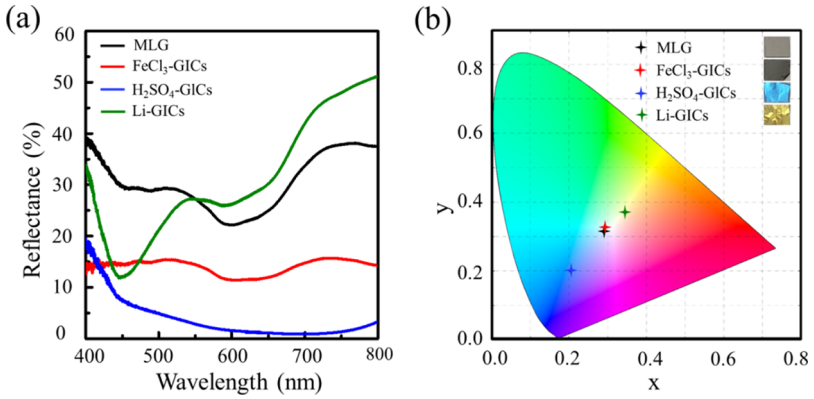

Figure 3. (a) Optical reflectance as a function of wavelength for pristine MLG before and after Li, $FeCl_3$, H_2SO_4 intercalation. (b) CIE 1931 chromaticity diagram of pristine MLG before and after Li, $FeCl_3$, H_2SO_4 intercalation. The black star represents pristine MLG with no intercalation. Green, blue, and red solid stars represent pristine MLG with Li, H_2SO_4, and $FeCl_3$ intercalation, respectively.

The colors that the human eye sees on the surface of the material are related to the reflected light. Figure 3a displays reflectance spectra of MLG film and GICs, with a wavelength range of 400−800 nm. The reflectance of pristine MLG film is between 22.16% (600 nm) and 37.50% (800 nm) with a valley at the wavelength of 600 nm. As to $FeCl_3$-GICs, it shows a significantly lower average reflectance compared to pristine MLG (from 37.50% down to 14.24% after $FeCl_3$ intercalation at 800 nm), with a weakening valley at 600 nm. Through H_2SO_4 intercalation, the whole reflectance is also reduced and is between 17.84% (400 nm) and 0.91% (700 nm), with a broad valley at the wavelength of 700 nm. After Li intercalation, the reflectance is found to exhibit a lower reflectance in the wavelength of 400−534 nm but a higher reflectance in the wavelength of 534−800 nm compared to pristine MLG. Additionally, there are two significant valleys generated at 450 and 600 nm. In a word, their reflectivity spectra change remarkably after intercalation, which is related to the color of materials.

Spectral reflectance is used to precisely calculate materials' color through a CIE 1931 chromaticity diagram. In CIE 1931 system, three kinds of colors such as red, green, and blue are used to represent the composition of any color. The real spectral color can be obtained through the combination of three artificial colors that are so-called tristimulus values (X, Y, Z). The chromaticity coordinates (x, y, z) can be calculated by taking the ratios of X, Y, and Z to the sum of three tristimulus values,[52] and it can be expressed as eq 1.

$$x = \frac{X}{X + Y + Z}$$
$$y = \frac{Y}{X + Y + Z}$$
$$z = \frac{Z}{X + Y + Z} \quad (1)$$

Because the three quantities (x, y, z) are made always to sum to "1".[52] Generally, (x, y) coordinates are used to represent the color. Figure 3 shows the CIE 1931 diagram of pristine MLG and GICs. Pristine MLG and $FeCl_3$-GICs show their adjacent location with (0.288718, 0.313887) and (0.290947, 0.326507) in the black area, respectively. The position of Li-GICs and H_2SO_4-GICs are located in (0.345962, 0.370433) at the yellow region and (0.203858, 0.200098) at the blue area in the color coordinate, respectively.

The lithium intercalation stages are described as shown in Figure 4a. To investigate these intercalation stages, optical images and reflectivity spectra are used to trace the survey. Compared to other substrates such as quartz and copper, the Ni-grown substrate makes a strong adhesion between the Ni-grown substrate and MLG film. The flatness of the MLG film can keep well during the Li intercalation process. As shown in Figure 4a, a reversible variety of colors are generated in the large-scale CVD-grown MLG film through a charge and discharge process. The voltage profile within the potential range of 3.0−0.05 V versus Li/Li^+ agrees well with the previous reports,[40] and the curves for the first three cycles (Figure S1) suggest a fully reversible charge and discharge process. In the process of voltage falling from 3.0 to 0.05 V, the color of MLG film changes from gray (before) to dark blue (stage-3), dark red (stage-2), and bright yellow (stage-1) in turn, as shown in Figure 4a. When the voltages are lower than 0.2 V, the color of evolution from gray to yellow is observed by further decreasing the voltage, accompanied by an obvious voltage plateau. These plateaus are corresponding to the intercalation stages, consistent with that of the reported works.[25,53,54] Details are provided in Figure S4 (Supporting Information). Simultaneously, the yellow color changes back to gray when the voltage increases to 3.0 V. Figure 4b displays the reflectance spectra of different representative stage colors for MLG films during the Li intercalation process, with the visible wavelength range of 400 to 800 nm. MLG films before Li intercalation show that the reflectance is between 9.15% (600 nm) and 17.60% (800 nm) with an unobvious valley generated in the wavelength of 600 nm. The presence of the electrolyte can cause additional light absorption, so the MLG film before Li intercalation in Figure 4b shows a lower reflectivity than the pristine MLG film in Figure 3a. During the lithiation stage, the reflectance spectrum of stage-3 (blue curve) shows from 3.08% (400 nm) to 7.59% (800 nm), and an imperceptible valley can be observed. When reaching the stage-2 phase (red line), the reflectance displays an enormous change with a broad valley being generated in the wavelength range from 450 to 600 nm, and is between 5.02% at 583 nm and 28.39% at 800 nm. As to full intercalation (stage-1), the reflectance (green line) exhibits a higher average reflectance than before Li Intercalation (from 17.60 to 51.17% at 800 nm after Li intercalation). Additionally, two valleys are generated at 450 and 600 nm. According to the

https://doi.org/10.1021/acsphotonics.1c01223
ACS Photonics XXXX, XXX, XXX−XXX

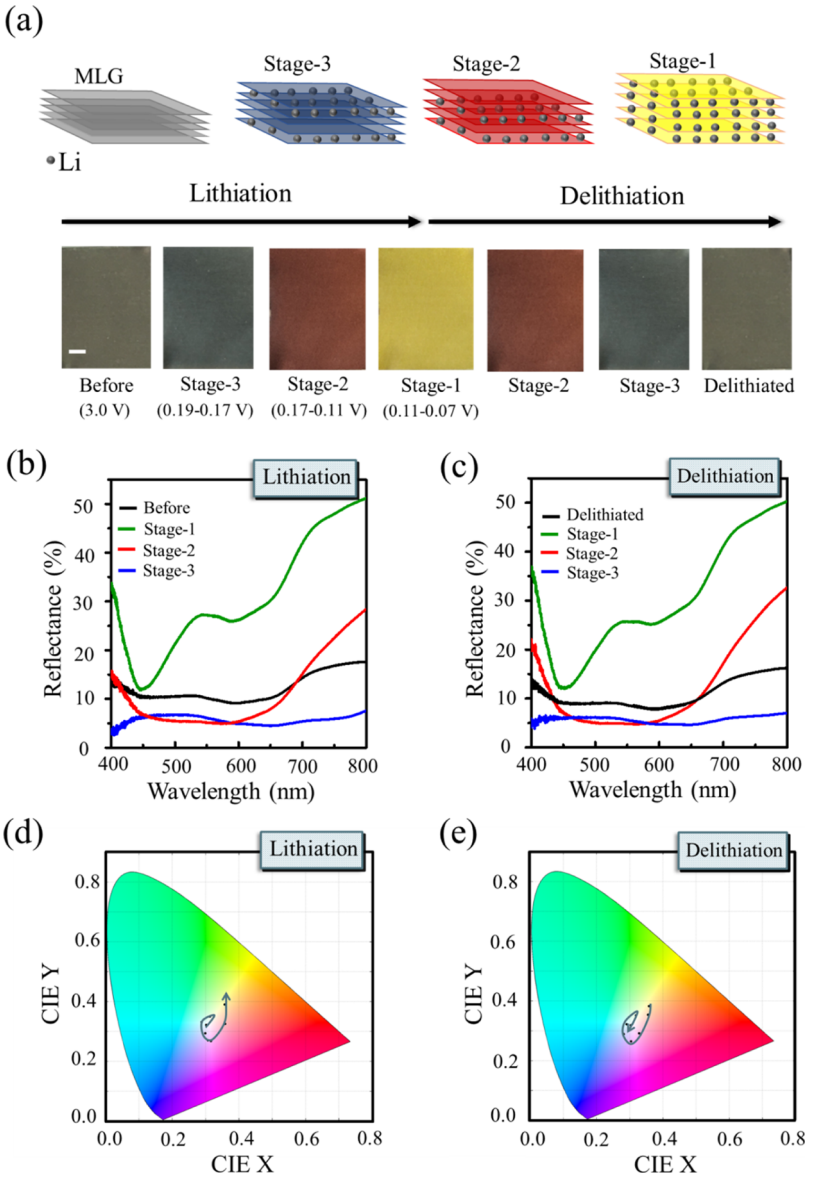

Figure 4. Stage transition is recorded during the electrochemical Li intercalation and de-intercalation process. (a) Schematic diagram of intercalation stages and optical images during Li intercalation and de-intercalation process. The scale bar is 2 mm. The electrode potential versus Li^+/Li is given for MLG before and after intercalation are given. MLG is grown on Ni foil. (b,c) are in situ optical reflectance as a function of wavelength for MLG film during Li intercalation and de-intercalation process. Black, green, blue, and red solid lines represent different intercalation stages of MLG. (d,e) are color evolution for MLG film during Li intercalation and de-intercalation process in the CIE 1931 chromaticity diagram.

CIE 1931 standard color-matching functions, the color evolution of coloration films during the Li intercalation process is demonstrated in the CIE chromaticity chart in Figure 4d, which displays the letter "e". In addition, during the de-intercalation process, not only optical images but also the reflectance, and the color evolution of coloration film in the CIE chromaticity chart are reversible as to the intercalation process, which dedicates a color change with good reversibility and non-volatility as shown in Figure 4a,c,e. In addition, LiC_6 encapsulated in air displays good stability without applied voltage, presenting the same yellow color and fully overlapped reflectivity spectra in seven days, shown in Figure S6.

Moreover, using the shadow mask, optical lithography, and argon plasma etching technique, the MLG film can be patterned into diverse shapes. Figure 5 shows a school logo of the National University of Defense Technology with dynamic color. During the Li intercalation process with a large current, different colors of dark blue, dark red, and bright yellow at different areas in the patterned MLG film can exist at the same time. The area close to the lithium plate is where the color changes first, as shown in the lithiation process in Figure 5. Because the lithium ions arrive with a shorter time to the position of MLG film near the lithium plate but with a longer time to the position of MLG film far from the lithium plate. Another reason for this phenomenon is that the intercalation starts at the edge of MLG film.[35] In the de-intercalation process, the yellow color turns into the different single colors with dark red, dark blue, and gray appearing successively, which can be achieved through a small constant current and suitable constant voltage. More pattern display is shown in Figure S7 (Supporting Information).

https://doi.org/10.1021/acsphotonics.1c01223
ACS Photonics XXXX, XXX, XXX−XXX

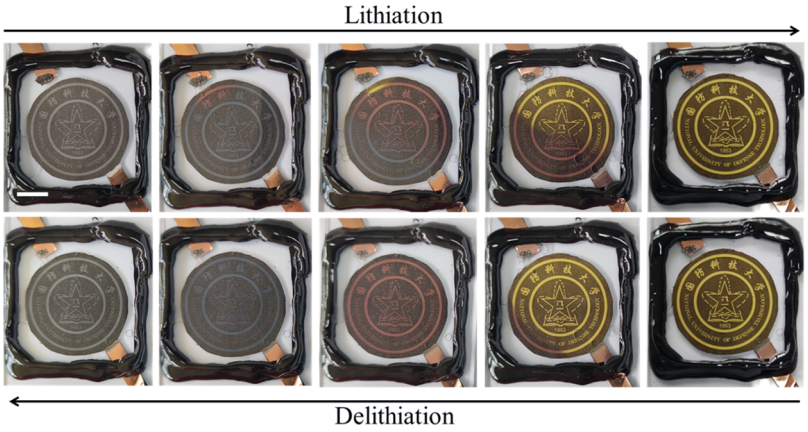

Figure 5. Color tuning of patterned MLG film during Li intercalation and de-intercalation process. The scale bar is 1 cm. The source of logo model is from https://baike.so.com/doc/5351215-5586672.html (Logo used with permission from Zhipeng Zhao on behalf of National University of Defense Technology).

CONCLUSIONS

In summary, we have successfully developed Li, H_2SO_4, and $FeCl_3$ intercalated MLG using an electrochemical, chemical, and thermal method. The color of MLG films is achieved from gray changing into bright yellow, deep blue, and dark, which is attributed to the variation of the band structure of graphene after intercalation with distinct reflectivity spectrum changing. Furthermore, consecutively tunable and non-volatile color modulation in a broad visible band can be achieved by an electrochemical optical platform. In addition, LiC_6 displays good stability without applied voltage, enabling convenience in practice appliances. Particularly, a reversible reading and erasing of complex patterns with various colors are also demonstrated. Our result provides a simple and effective method to dynamically tune 2D materials coloration, which shows excellent potential for specular reflection, sensing, anti-counterfeiting, displaying, and sensors.

METHODS

Preparation of MLG Film. About 50 nm CVD-grown MLG on a Ni foil (Nanjing MKNANO, China) was floated on a $FeCl_3$ etched aqueous solution surface (Aladdin Industrial Corporation, Shanghai, China). Several hours later, a free-standing MLG film was acquired and transferred to deionized water to remove the residual $FeCl_3$. Next, the MLG film was transferred onto a quartz plate and baked in an oven at 80 °C to dry the remaining water.

Preparation of Li-GICs. Device fabrication: Two Cu electrodes were attached to a 0.5 mm quartz plate. CVD MLG films on Ni foil were transferred to a Cu electrode nearly and contacted with a conductive silver paste. Then, the device was transferred inside a glovebox (Lab2000, Etelux, China) filled with an argon atmosphere. Subsequently, the Li pellet was deposited onto an isolated Cu electrode. After that, we covered a quartz plate on the graphite film and Li pellet areas, epoxy was used to seal three edges, a small pocket was created and filled with electrolyte ($LiPF_6$ in ethylene carbonate/diethyl carbonate, w/w = 1:1). Lastly, the pocket with epoxy was sealed to prevent oxidation.

Electrochemical intercalation and deintercalation: The intercalation and deintercalation processes were controlled by the Vertex One electrochemical workstation (Ivium Technologies, The Netherlands). Constant current charge and discharge were set as 5 μA. Then, 50 mV of constant voltage was kept for enough time to get fully lithiated graphite LiC_6.

Preparation of H_2SO_4-GICs. $(NH_4)_2S_2O_8$ (1.0 g, Sigma-Aldrich) was added to 96–98% H_2SO_4 (10.0 ml) with constant swirling. After 10 min, $(NH_4)_2S_2O_8$ was completely dissolved, accompanied by gases production from the partial decomposition of the persulfate anion. Then, the preparation of a MLG film was dropped by a drop of the mixing solution and covered with a quartz plate. A few minutes later, the formation of H_2SO_4-GICs was synthesized with the appearance of the deep blue color of MLG films. To deintercalation, the $(NH_4)_2S_2O_8$-H_2SO_4 solution surrounding the MLG film was diluted with deionized water.

Preparation of $FeCl_3$-GICs. The getting MLG film and anhydrous $FeCl_3$ powder (Alfa Aesar, 98%) were positioned in different zones inside a quartz tube, then sealed the tube with epoxy, all manipulations were performed in an argon-filled glovebox, restraining anhydrous $FeCl_3$ powder from moisture. After the epoxy was completely dry, the tube was transferred out of the glovebox to air. Subsequently, the MLG film and the $FeCl_3$ powder were heated for 24 h at 360 and 310 °C, respectively.

Optical and Electrical Characterization. The samples were characterized using a confocal Raman microscope (Witec Alpha-300R) equipped with a solid-state Nd^+:YAG exciting laser (532 nm) and XRD (Rigaku, Japan) with a Cu Kα source (λ = 1.5406 Å) to analyze the phases composition and structural parameters. XRD spectra were measured with a step of 0.02°. The Li-GIC sample was disassembled from a reaction cell and sealed inside XRD special test glass slot by the Kapton tape, the manipulations were all carried out inside the glovebox. The sheet resistance of a 50 nm thick MLG film and GICs samples was measured by the van der Pauw method, using a Keithley 2636B source meter (Tektronix, USA).

Reflection Measurement and Color Calculation. The reflectance of the MLG film before and after intercalation was tested by an angle-resolved spectrum system (Ideaoptics, China). Calculation of colors by two normalized values (x and y) derived from the tristimulus values was carried out, measuring the response of human eyes to the light based on the CIE 1931 color space..

https://doi.org/10.1021/acsphotonics.1c01223
ACS Photonics XXXX, XXX, XXX−XXX

■ ASSOCIATED CONTENT

Supporting Information

The Supporting Information is available free of charge at https://pubs.acs.org/doi/10.1021/acsphotonics.1c01223.

Additional details on the voltage profile of graphene film during multiple Li charge and discharge processes, and the film color evolution with the variation of voltage plateau during Li intercalation process; in situ resistance of MLG during the H_2SO_4 intercalation and de-intercalation process; demonstration the mechanism of intercalation change color; encapsulated LiC_6 film device for XRD test; stability of encapsulated LiC_6 device; and snow flower patterns color display (PDF)

Li intercalation process movie of a graphene film (AVI)

Li de-intercalation process movie of a graphene film (AVI)

H_2SO_4 intercalation process movie of a graphene film (AVI)

H_2SO_4 de-intercalation process movie of a graphene film (AVI)

■ AUTHOR INFORMATION

Corresponding Authors

Renyan Zhang − *College of Advanced Interdisciplinary Studies, National University of Defense Technology, Changsha 410073, China; State Key Laboratory of Optical Technologies for Microfabrication, Institute of Optics and Electronics, Chinese Academy of Sciences, Chengdu 610209, China;* orcid.org/0000-0001-6949-8888; Email: ryancms@sina.cn

Tian Jiang − *College of Advanced Interdisciplinary Studies, National University of Defense Technology, Changsha 410073, China; Beijing Institute for Advanced Study, National University of Defense Technology, Beijing 100020, China;* orcid.org/0000-0003-3343-5548; Email: tjiang@nudt.edu.cn

Authors

Ganying Zeng − *College of Advanced Interdisciplinary Studies, National University of Defense Technology, Changsha 410073, China; Beijing Institute for Advanced Study, National University of Defense Technology, Beijing 100020, China*

Yinlong Tan − *College of Advanced Interdisciplinary Studies, National University of Defense Technology, Changsha 410073, China; Beijing Institute for Advanced Study, National University of Defense Technology, Beijing 100020, China;* orcid.org/0000-0002-3815-3075

Xiang'ai Cheng − *Beijing Institute for Advanced Study, National University of Defense Technology, Beijing 100020, China*

Complete contact information is available at: https://pubs.acs.org/10.1021/acsphotonics.1c01223

Notes

The authors declare no competing financial interest.

■ ACKNOWLEDGMENTS

This work was supported by the National Natural Science Foundation of China (NSFC) (grant nos. 62075240, 61801498); the Scientific Researches Foundation of National University of Defense Technology (grant no. ZK18-01-03); the fellowship of China Postdoctoral Science Foundation (grant no. 2020T130654), the China Postdoctoral Science Foundation (CPSF) (grant no. 2019M663569); International Cooperation on Scientific and Technological Innovation of Sichuan province (grant no. 2020YFH0004).

■ REFERENCES

(1) Duan, X.; Kamin, S.; Liu, N. Dynamic plasmonic colour display. *Nat. Commun.* **2017**, *8*, 14606.

(2) Li, H.; McRae, L.; Firby, C. J.; Elezzabi, A. Y. Rechargeable aqueous electrochromic batteries utilizing ti-substituted tungsten molybdenum oxide based Zn^{2+} Ion Intercalation Cathodes. *Adv. Mater.* **2019**, *31*, 1807065.

(3) Ergoktas, M. S.; Bakan, G.; Kovalska, E.; Le Fevre, L. W.; Fields, R. P.; Steiner, P.; Yu, X.; Salihoglu, O.; Balci, S.; Fal'ko, V. I.; Novoselov, K. S.; Dryfe, R. A. W.; Kocabas, C. Multispectral graphene-based electro-optical surfaces with reversible tunability from visible to microwave wavelengths. *Nat. Photonics* **2021**, *15*, 493−498.

(4) Isapour, G.; Lattuada, M. Bioinspired Stimuli-responsive color-changing systems. *Adv. Mater.* **2018**, *30*, 1707069.

(5) Bullett, T. R. *Appearance Qualities of Paint-Basic Concepts*; Woodhead publishing, 1999, pp 621−641.

(6) Sekar, N. *Optical Effect Pigments for Technical Textile Applications*; Woodhead Publishing, 2013; Vol. *37*−*46*.

(7) Yue, W.; Gao, S.; Lee, S. S.; Kim, E. S.; Choi, D. Y. Highly reflective subtractive color filters capitalizing on a silicon metasurface integrated with nanostructured aluminum mirrors. *Laser Photonics Rev.* **2017**, *11*, 1600285.

(8) Wang, Y.; Zheng, M.; Ruan, Q.; Zhou, Y.; Chen, Y.; Dai, P.; Yang, Z.; Lin, Z.; Long, Y.; Li, Y.; Liu, N.; Qiu, C.-W.; Yang, J. K. W.; Duan, H. Stepwise-nanocavity-assisted transmissive color filter array microprints. *Research* **2018**, *2018*, 8109054.

(9) Liu, B.; Rasines Mazo, A.; Gurr, P. A.; Qiao, G. G. Reversible nontoxic thermochromic microcapsules. *ACS Appl. Mater. Interfaces* **2020**, *12*, 9782−9789.

(10) Yang, J.; Tang, C.; Sun, H.; Liu, Z.; Liu, Z.; Li, K.; Zhu, L.; Qin, G.; Sun, G.; Li, Y.; Chen, Q. Tough, transparent, and anti-freezing nanocomposite organohydrogels with photochromic properties. *ACS Appl. Mater. Interfaces* **2021**, *13*, 31180−31192.

(11) Zhang, G.; Hu, J.; Nie, Y.; Zhao, Y.; Wang, L.; Li, Y.; Liu, H.; Tang, L.; Zhang, X.; Li, D.; Sun, L.; Duan, H. Integrating flexible ultralight 3D Ni micromesh current collector with Nico bimetallic hydroxide for smart hybrid supercapacitors. *Adv. Funct. Mater.* **2021**, *31*, 2100290.

(12) Sun, S.; Yang, W.; Zhang, C.; Jing, J.; Gao, Y.; Yu, X.; Song, Q.; Xiao, S. Real-time tunable colors from microfluidic reconfigurable all-dielectric metasurfaces. *ACS Nano* **2018**, *12*, 2151−2159.

(13) Li, J.; Chen, Y.; Hu, Y.; Duan, H.; Liu, N. Magnesium-based metasurfaces for dual-function switching between dynamic holography and dynamic color display. *ACS Nano* **2020**, *14*, 7892−7898.

(14) Zhu, J.; Yu, Z.; Burkhard, G. F.; Hsu, C.-M.; Connor, S. T.; Xu, Y.; Wang, Q.; McGehee, M.; Fan, S.; Cui, Y. Optical absorption enhancement in amorphous silicon nanowire and nanocone arrays. *Nano Lett.* **2009**, *9*, 279−282.

(15) Zeng, B.; Gao, Y.; Bartoli, F. J. Ultrathin nanostructured metals for highly transmissive plasmonic subtractive color filters. *Sci. Rep.* **2013**, *3*, 2840.

(16) Kumar, K.; Duan, H.; Hegde, R. S.; Koh, S. C. W.; Wei, J. N.; Yang, J. K. W. Printing colour at the optical diffraction limit. *Nat. Nanotechnol.* **2012**, *7*, 557−561.

(17) Daqiqeh Rezaei, S.; Dong, Z.; You En Chan, J.; Trisno, J.; Ng, R. J. H. Nanophotonic structural colors. *ACS Photonics* **2021**, *8*, 18−33.

(18) Neubrech, F.; Duan, X.; Liu, N. Dynamic plasmonic color generation enabled by functional materials. *Sci. Adv.* **2020**, *6*, No. eabc2709.

(19) Rossi, S.; Olsson, O.; Chen, S.; Shanker, R.; Banerjee, D.; Dahlin, A.; Jonsson, M. Dynamically tuneable reflective structural

coloration with electroactive conducting polymer nanocavities. *Adv. Mater.* **2021**, 2105004.
(20) Chen, S.; Rossi, S.; Shanker, R.; Cincotti, G.; Gamage, S.; Kühne, P.; Stanishev, V.; Engquist, I.; Berggren, M.; Edberg, J.; Darakchieva, V.; Jonsson, M. P. Tunable structural color images by UV-Patterned conducting polymer nanofilms on metal surfaces. *Adv. Mater.* **2021**, *33*, 2102451.
(21) Gao, Y.; Huang, C.; Hao, C.; Sun, S.; Zhang, L.; Zhang, C.; Duan, Z.; Wang, K.; Jin, Z.; Zhang, N.; Kildishev, A. V.; Qiu, C.-W.; Song, Q.; Xiao, S. Lead halide perovskite nanostructures for dynamic color display. *ACS Nano* **2018**, *12*, 8847−8854.
(22) Chen, Y.; Duan, X.; Matuschek, M.; Zhou, Y.; Neubrech, F.; Duan, H.; Liu, N. Dynamic color displays using stepwise cavity resonators. *Nano Lett.* **2017**, *17*, 5555−5560.
(23) Arsenault, A. C.; Puzzo, D. P.; Manners, I.; Ozin, G. A. Photonic-crystal full-colour displays. *Nat. Photonics* **2007**, *1*, 468−472.
(24) Lee, Y.; Yun, J.; Seo, M.; Kim, S. J.; Lee, B. Full-color-tunable nanophotonic device using electrochromic tungsten trioxide thin film. *Nano Lett.* **2020**, *20*, 6084−6090.
(25) Bao, W.; Wan, J.; Han, X.; Cai, X.; Zhu, H.; Kim, D.; Ma, D.; Xu, Y.; Munday, J. N.; Drew, H. D.; Fuhrer, M. S.; Hu, L. Approaching the limits of transparency and conductivity in graphitic materials through lithium intercalation. *Nat. Commun.* **2014**, *5*, 4224.
(26) Bointon, T. H.; Khrapach, I.; Yakimova, R.; Shytov, A. V.; Craciun, M. F.; Russo, S. Approaching magnetic ordering in graphene materials by $FeCl_3$ Intercalation. *Nano Lett.* **2014**, *14*, 1751−1755.
(27) Yao, J.; Koski, K. J.; Luo, W.; Cha, J. J.; Hu, L.; Kong, D.; Narasimhan, V. K.; Huo, K.; Cui, Y. Optical transmission enhacement through chemically tuned two-dimensional bismuth chalcogenide nanoplates. *Nat. Commun.* **2014**, *5*, 5670.
(28) Zhang, R.; Waters, J.; Geim, A. K.; Grigorieva, I. V. Intercalant-independent transition temperature in superconducting black phosphorus. *Nat. Commun.* **2017**, *8*, 15036.
(29) Ahamd, H. M. R.; Zhou, J. Intercalation induced ferromagnetism in group-V transition metal dichalcogenide bilayer. *AIP Adv.* **2020**, *10*, 045323.
(30) Kappera, R.; Voiry, D.; Yalcin, S. E.; Branch, B.; Gupta, G.; Mohite, A. D.; Chhowalla, M. Phase-engineered low-resistance contacts for ultrathin MoS_2 transistors. *Nat. Mater.* **2014**, *13*, 1128−1134.
(31) Tchougréeff, A. L. Charge density wave state of monolayers in graphite intercalation compounds. *J. Phys. Chem.* **1996**, *100*, 14048−14055.
(32) Wan, J.; Xu, Y.; Ozdemir, B.; Xu, L.; Sushkov, A. B.; Yang, Z.; Yang, B.; Drew, D.; Barone, V.; Hu, L. Tunable broadband nanocarbon transparent conductor by electrochemical intercalation. *ACS Nano* **2017**, *11*, 788−796.
(33) Zhao, L.; Zhang, R.; Deng, C.; Peng, Y.; Jiang, T. Tunable infrared emissivity in multilayer graphene by ionic liquid intercalation. *Nanomaterials* **2019**, *9*, 1096.
(34) Salihoglu, O.; Uzlu, H. B.; Yakar, O.; Aas, S.; Balci, O.; Kakenov, N.; Balci, S.; Olcum, S.; Süzer, S.; Kocabas, C. Graphene-based adaptive thermal camouflage. *Nano Lett.* **2018**, *18*, 4541−4548.
(35) Zeng, G.; Zhang, R.; Sui, Y.; Li, X.; OuYang, H.; Pu, M.; Chen, H.; Ma, X.; Cheng, X. a.; Yan, W.; Xu, M.; Hong, M.; Jiang, T.; Luo, X. Inversion symmetry breaking in lithium intercalated graphitic materials. *ACS Appl. Mater. Interfaces* **2020**, *12*, 28561−28567.
(36) Zhang, C.; Zeng, G.; Zhang, R.; Tang, Y.; Liu, Q.; Jiang, T. Tunable nonlinear optical responses of few-layer graphene through lithium intercalation. *Nanophotonics* **2021**, *10*, 2661−2669.
(37) Dimiev, A. M.; Bachilo, S. M.; Saito, R.; Tour, J. M. Reversible formation of ammonium persulfate/sulfuric acid graphite intercalation compounds and their peculiar Raman spectra. *ACS Nano* **2012**, *6*, 7842−7849.
(38) Stark, M.; Kuntz, K.; Martens, S.; Warren, S. Intercalation of layered materials from bulk to 2D. *Adv. Mater.* **2019**, *31*, 1808213.
(39) Reich, S.; Thomsen, C. Raman spectroscopy of graphite. *Philos. Trans. R. Soc., A* **2004**, *362*, 2271−2288.
(40) Li, Y.; Lu, Y.; Adelhelm, P.; Titirici, M.-M.; Hu, Y.-S. Intercalation chemistry of graphite: alkali metal ions and beyond. *Chem. Soc. Rev.* **2019**, *48*, 4655−4687.
(41) Qi, X.; Qu, J.; Zhang, H.-B.; Yang, D.; Yu, Y.; Chi, C.; Yu, Z.-Z. $FeCl_3$ intercalated few-layer graphene for high lithium-ion storage performance. *J. Mater. Chem. A* **2015**, *3*, 15498−15504.
(42) Zhao, W.; Tan, P. H.; Liu, J.; Ferrari, A. C. Intercalation of few-layer graphite flakes with $FeCl_3$: Raman determination of Fermi level, layer by layer decoupling, and stability. *J. Am. Chem. Soc.* **2011**, *133*, 5941−5946.
(43) Dimiev, A. M.; Ceriotti, G.; Behabtu, N.; Zakhidov, D.; Pasquali, M.; Saito, R.; Tour, J. M. Direct real-time monitoring of stage transitions in graphite intercalation compounds. *ACS Nano* **2013**, *7*, 2773−2780.
(44) Sun, Y.; Han, F.; Zhang, C.; Zhang, F.; Zhou, D.; Liu, H.; Fan, C.; Li, X.; Liu, J. $FeCl_3$ intercalated microcrystalline graphite enables high volumetric capacity and good cycle stability for lithium-ion batteries. *Energy Technol.* **2019**, *7*, 1801091.
(45) Song, X. Y.; Kinoshita, K.; Tran, T. D. Microstructural characterization of lithiated graphite. *J. Electrochem. Soc.* **1996**, *143*, L120−L123.
(46) Moissette, A.; Fuzellier, H.; Burneau, A.; Dubessy, J.; Lelaurain, M. Sulfate graphite intercalation compounds: new electrochemical data and spontaneous intercalation. *Carbon* **1995**, *33*, 123−128.
(47) Bouayad, B.; Marrouche, A.; Tihli, M.; Fuzellier, H.; Metrot, A. Insertion d'acides mineraux dans le graphite: etude du systeme graphite-SO_3H_2O. *Synth. Met.* **1983**, *7*, 159−165.
(48) Metrot, A.; Fischer, J. Charge transfer reactions during anodic oxidation of graphite in H_2SO_4. *Synth. Met.* **1981**, *3*, 201−207.
(49) Bouayad, B.; Fuzellier, H.; Lelaurain, M.; Metrot, A.; Rousseaux, F. Modifications structurales observees en fonction de la charge pour les composes de premiere et deuxieme stades graphite-acide sulfurique. *Synth. Met.* **1983**, *7*, 325−331.
(50) Kanetani, K.; Sugawara, K.; Sato, T.; Shimizu, R.; Iwaya, K.; Hitosugi, T.; Takahashi, T. Ca intercalated bilayer graphene as a thinnest limit of superconducting C_6Ca. *Proc. Natl. Acad. Sci. U.S.A.* **2012**, *109*, 19610−19613.
(51) Zhan, D.; Sun, L.; Ni, Z. H.; Liu, L.; Fan, X. F.; Wang, Y.; Yu, T.; Lam, Y. M.; Huang, W.; Shen, Z. X. $FeCl_3$-based few-Layer graphene intercalation compounds: single linear dispersion electronic band structure and strong charge transfer doping. *Adv. Funct. Mater.* **2010**, *20*, 3504−3509.
(52) Krishnaiah, K. V.; Kumar, K. U.; Jayasankar, C. K. Spectroscopic properties of Dy^{3+}-doped oxyfluoride glasses for white light emitting diodes. *Mater. Express* **2013**, *3*, 61−70.
(53) Ohzuku, T.; Iwakoshi, Y.; Sawai, K. Formation of lithium-graphite intercalation compounds in nonaqueous electrolytes and their application as a negative electrode for a lithium ion (Shuttlecock) cell. *J. Electrochem. Soc.* **1993**, *140*, 2490−2498.
(54) Shellikeri, A.; Watson, V.; Adams, D.; Kalu, E. E.; Read, J. A.; Jow, T. R.; ZhengZheng, J. S. J. P. Investigation of pre-lithiation in graphite and hard-carbon anodes using different lithium source structures. *J. Electrochem. Soc.* **2017**, *164*, A3914−A3924.

https://doi.org/10.1021/acsphotonics.1c01223
ACS Photonics XXXX, XXX, XXX−XXX